Journal of Membrane Science 527 (2017) 35–42

Contents lists available at ScienceDirect

Journal of Membrane Science

journal homepage: www.elsevier.com/locate/memsci

# Synthesis of PVDF-g-PSSA proton exchange membrane by ozone-induced graft copolymerization and its application in microbial fuel cells

Chen Li, Lei Wang*, Xudong Wang, Mengxiao Kong, Quan Zhang, Guangyuan Li

*Key Laboratory of Membrane Separation of Shaanxi Province, School of Environmental & Municipal Engineering, Xi'an University of Architecture and Technology, Yan Ta Road. No.13, Xi'an 710055, China*

ARTICLE INFO

*Keywords:*
Proton exchange membrane
Graft copolymerization
Membrane fouling
Quartz crystal microbalance with dissipation monitoring
Microbial fuel cells

ABSTRACT

Thermally induced graft copolymerization of sodium styrene sulfonate (SSS) with ozone-preactivated poly(-vinylidene fluoride) (PVDF) produced a PVDF-g-PSSS copolymer. Sulfonic acid proton exchange membranes (PVDF-g-PSSA) were then prepared using the solvent evaporation method. They were investigated with a Fourier transform infrared spectrometer and an X-ray diffractometer. The results indicate that the proton conductivity of the prepared membranes reached 0.046 S/cm when the degree of grafting was 50.52%. Results from a quartz crystal microbalance with dissipation monitoring indicated that the PVDF-g-PSSA membrane showed superior antifouling performance to that of a Nafion membrane. The performance of the prepared membrane in dual-chamber microbial fuel cells was also evaluated and compared with that of Nafion 117. Although the microbial fuel cell with the prepared membrane generated lower maximum power density (106.7 mW/m$^2$) than that with Nafion 117 (132.0 mW/m$^2$), it was more cost-effective because of its lower price and more simplified preparation process. In addition, its chemical oxygen demand (COD) removal (85%) was much higher than that of Nafion 117 (74%).

## 1. Introduction

It is well known that global fossil fuels will run out in the near future. With increasing concerns about pollution of the atmosphere and global warming caused by fossil fuel combustion, as well as the increasing need for sustainable energy, many scientists have committed to finding renewable and alternative sources of energy [1,2]. Microbial fuel cells (MFCs) are considered a novel process for alternative energy generation and have attracted wide-ranging interest because they can extract electricity from diverse organic wastes while providing treatment of wastewater [3,4].

An MFC basically consists of two electrodes, the anode and cathode, that are commonly separated by a proton exchange membrane (PEM). Under anaerobic conditions, the substrate is oxidized by microorganisms attached to the anode to generate electrons and protons. The electrons and protons transfer and migrate through an external circuit and a PEM, respectively, toward the cathode, where they react with oxygen to form water [5,6]. MFCs show great promise for broad applications in wastewater treatment. However, low-scale power density production and high cost have become the greatest obstacles to their use. The PEM used to separate the anode and cathode is a critical component of the MFC, as it has a significant influence on its performance and overall cost. The membranes should allow protons to transport easily from anode to cathode, while preventing the transfer of oxygen and substrates [7,8]. Nafion membrane is still considered to be the best membrane for MFCs because of its high proton conductivity, as well as its excellent chemical and electrochemical properties. However, several problems, including its high cost, oxygen leakage, and substrate loss, are limiting factors for MFCs applications [9]. In addition, biofouling will occur during long-term operation of MFCs, because biofilms can be formed on the surface of the membrane, which will reduce the performance of the fuel cell [10]. Xu et al. reported their MFCs suffered badly from biofouling during three months' operation, resulting in degraded performance because of the physical blockage of cation transfer and limitations on proton transfer [11]. Miskan et al. found that the extension of the operating time of the MFC promoted the growth of the biofouling layer on the membrane and the biofouling layer thickness exceeded 250 μm after six months' operation, which led to a significant increase in membrane resistance and eventually reduced MFC performance [12]. Thus, an anti-biofouling membrane with good proton conductivity is essential for the long-term operation and large-scale practical application of MFCs.

Poly(vinylidene fluoride) (PVDF) has been widely used in battery field, because of its excellent chemical resistance, good thermal

* Corresponding author.
*E-mail address:* wl0178@126.com (L. Wang).

http://dx.doi.org/10.1016/j.memsci.2016.12.065
Received 12 August 2016; Received in revised form 20 December 2016; Accepted 26 December 2016
Available online 05 January 2017

stability, and outstanding mechanical properties [13–15]. Lehtinen et al. prepared sulfonic acid proton exchange membranes using a radiation-grafting technique, and they found that PVDF-g-PSSA membranes have a higher proton conductivity than Nafion membranes [16]. Qiu et al. reported a method of preparing a PVDF-g-PSSA membrane using a solution-grafting technique [17]. These membranes were prepared in two steps, namely grafting of styrene onto pretreated PVDF films followed by sulfonation to confer proton-conducting sites [18]. However, the sulfonation reaction may damage the physical strength and surface topography of pretreated membranes and the degree of sulfonation of prepared membranes was difficult to control. In addition, these processes are complicated and expensive [19]. Nasef et al. reported a single-step method for preparation of PVDF-g-PSSA by grafting sodium styrene sulfonate (SSS) onto electron beam-irradiated PVDF [20]. The direct preparation of membranes using SSS eliminated the hazardous sulfonation reaction and could simplify the casting process and reduce costs. However, this method of surface grafting onto existing PVDF membranes has some inherent drawbacks. For instance, it is very difficult to control the degree of grafting, so the extent of grafting on the membrane surfaces may differ considerably. Furthermore, the grafting process may be severely limited in the interior of the membrane. Therefore, the concept of producing functional graft copolymers prior to membrane preparation may prove to be a better alternative in certain cases [21]. Directly using functional graft copolymers can yield functionalized membranes with uniform and homogeneous graft distribution through control of copolymer composition and casting conditions. Compared with other surface modification techniques, ozone pretreatment of PVDF to introduce peroxides, followed by thermally initiated radical graft copolymerization, is a cost-effective method [22,23].

In the present work, PVDF-g-SSS copolymer was produced via thermally induced graft copolymerization of SSS with ozone-preactivated PVDF. Then, sulfonic acid proton exchange membranes were fabricated using the solvent evaporation method. The effects of the mass ratio of PVDF/SSS on the water uptake, proton conductivity, and swelling ratio of the obtained membranes were evaluated. The anti-fouling property of the membrane and the membrane fouling mechanism were studied at the microlevel using a quartz crystal microbalance with dissipation monitoring (QCM-D). The performance of the prepared membrane in an MFC was also investigated and compared with that of Nafion 117.

## 2. Materials and methods

### 2.1. Fabrication of PVDF-g-PSSA membranes

2.0 g of PVDF polymer (Solef 6020; Solvay Advanced Polymers Co., USA) and different quality of SSS powder (2.0, 4.0, 6.0, 8.0 and 10.0 g, respectively; Aladdin, Shanghai, China) were dissolved in 30 ml of N-methyl pyrrolidone (NMP; Fucheng Chemical Reagent Co., China) and 30 ml of dimethyl sulfoxide (DMSO; Fucheng Chemical Reagent Co., China), respectively. The mass ratio of PVDF/SSS was controlled in the range of 1:1 to 1:5. A continuous stream of $O_3/O_2$ mixture was bubbled through 30 ml of PVDF/NMP solution at room temperature (25 °C) for 8 min. The flow rate was adjusted to 50 L/h to give an ozone concentration of 0.08–0.12 g/L in the gaseous mixture. After ozone pretreatment, the polymer solution was cooled in an ice bath. The activated PVDF solution was degassed with a nitrogen stream for 30 min to remove any ozone and oxygen dissolved in the solution. Subsequently, the nitrogen-bubbled SSS/DMSO solution and 0.01 g benzoyl peroxide (BPO; Fucheng Chemical Reagent Co., China) initiator were added to the reaction mixture in a three-necked flask. The three-necked flask was stirred at 80 °C in a water bath to induce the BPO pyrolysis and to initiate the radical graft copolymerization of SSS. The reaction was allowed to proceed for 4 h under a constant flow of nitrogen. The reaction mixture was then cooled and the resultant PVDF-g-PSSS copolymer was precipitated in pure methanol. After filtration, the copolymer was washed with methanol and water several times to remove the homopolymer and the un-reacted monomer. The copolymer sample was dried at 60 °C for 24 h. The degree of grafting of the prepared PVDF-g-PSSS copolymer was determined by acid–base back titration [24].

The PVDF-g-PSSA membrane was prepared using a solvent evaporation method. 5.0 g of PVDF-g-PSSS copolymer with different degree of grafting was dissolved in 95 ml of NMP to a concentration of 5 wt% at 60 °C. The copolymer solution was spread as a liquid film onto a glass plate prepared in our laboratory in an amount that would give a thickness of ca. 100 μm of the formed membrane. Solvent was then evaporated at 60 °C for 2 h, then at 80 °C until the casting solution became a solid membrane. The membrane was then soaked in deionized water to remove any residual solvent. Finally, the membrane was converted to $H^+$ form by treating with 1 M HCL solution for 24 h. PVDF membranes were prepared using the same method, except that the membranes obtained did not require treatment with HCL solution.

### 2.2. Membrane characterization

The chemical structures of the PVDF-g-PSSA membranes and PVDF membranes were examined using a Fourier transform infrared spectrometer (FTIR; IRPrestige-21, Shimadzu, Japan). Membrane samples were scanned 40 times with 4 $cm^{-1}$ resolution in the range of 400–4000 $cm^{-1}$ in transmittance mode. The crystal structure of the PVDF-g-PSSA membranes and PVDF membranes was measured using an X-ray diffractometer (XRD; Ultima IV, Rigaku Co Ltd., Japan). The diffractograms were collected at ambient temperature in the scanning range of $2\theta$=5–80° using Cu Ka radiation.

The thermal stability of the PVDF-g-PSSA membrane was studied by thermal gravity analysis (TGA; STA 449F3, Netzsch, Germany). The samples were heated from 40 °C to about 700 °C at a rate of 10 °C/min under the nitrogen atmosphere.

The water uptake (wt%) evaluates the amount of water confined within the membrane [25]. The swollen equilibrium samples in deionized water at room temperature were removed and the excess water adhering to their surfaces was quickly wiped by blotting paper and the membrane weighed. The water uptake of the membrane was determined from the difference in weight between dried and fully hydrated membranes as:

$$wt\% = \frac{W_w - W_d}{W_d} \times 100\%, \quad (1)$$

where $W_\omega$ and $W_d$ are the weight of the fully hydrated membrane and the dried membrane, respectively.

The swelling ratio (ΔS%) assesses the dimensional stability of a membrane in the target solvent. The membranes were immersed in deionized water at room temperature for 24 h. Then the surface areas of the dried and fully hydrated membrane samples were measured [26]. The swelling ratio of the membrane was calculated by:

$$\Delta S\% = \frac{S_w - S_d}{S_d} \times 100\%, \quad (2)$$

where $S_\omega$ and $S_d$ are the surface area of the fully hydrated membrane sample and the dried membrane sample, respectively. The breaking strength of the prepared membranes were measured by tension tester (LJ-5000N, Chengde, Hebei). The sample size was 1 cm×8 cm and all the samples were measured at room temperature (25 °C) with a stretching speed of 20 mm/min. The reported values were averages of at least five measurements.

The contact angle measurements of membranes were conducted using a contact angle measurement system (OCA20, DataPhysics, Germany). The membrane samples were fixed onto the slides and dried. Then 5 μL of water was dropped on the membrane surface from a microsyringe with a stainless steel needle at room temperature. The

contact angle of a membrane sample was determined as the average value of at least five measurements of drops at different locations [27].

The proton conductivity (σ) of the membranes was measured using an AC impedance technique by an electrochemical workstation (PAR2273, AMT, USA). Impedance spectra were recorded in the frequency range of $2\times10^{6}$ Hz to $5\times10^{-2}$ Hz. A two-probe conductivity cell similar to that employed by Zawodzinski et al. [28] was used to host the membrane samples [29]. The cell was immersed in water and measured the AC impedance spectroscopy of the fully hydrated membranes. The resistance of the membrane was taken at the intercept of the impedance curve with the real axis at the high-frequency end. The proton conductivity of the membranes was calculated by:

$$\sigma = \frac{a}{R_m \times A}, \tag{3}$$

where $a$ is the distance between the two electrodes, $R_m$ is the resistance of the membrane, and $A$ is the cross-sectional area of the membrane.

### 2.3. QCM-D experiments

In the present study, BSA (98% purity, Sigma-Aldrich, St. Louis, MO), one of the most widely used model proteins for membrane fouling, was selected. QCM-D combined with a membrane-coated sensor crystal was used to investigate the deposition and adsorption behavior of BSA dissolved in either ultrapure water (UP; Elga, UK) or PBS buffer solution (50 mM) on the PVDF-g-PSSA and Nafion surfaces and the structure of the BSA adsorption layers. The adherence of the BSA on the different membranes was carried out in a QCM-D system (E1, Q-Sense, Sweden) by monitoring the change in the oscillation frequency ($\Delta f$) of the membrane-coated quartz crystal sensor.

First, a PVDF-g-PSSA or Nafion membrane was formed on the surface of a silica-coated sensor crystal (QSX 301 silica, Q-Sense). To prepare a PVDF-g-PSSA-coated sensor crystal, the PVDF-g-PSSS copolymer was first converted to $H^+$ form. A homogeneous PVDF-g-PSSA solution was prepared by dissolving PVDF-g-PSSA in N,N/-dimethylacetamide (DMAc; Fuchen Chemical Reagent Co., China) to a concentration of 5 wt% at 60 °C. The silica-coated crystal sensors with a fundamental resonant frequency of 4.95 Hz were cleaned using 10% (w/v) sodium dodecyl sulfate and then rinsed thoroughly with ultrapure water and dried with pure $N_2$ gas. The cleaned silica-coated sensor crystal was fixed on the rotary platform of a spin coater (KW-4A; Institute of Microelectronics of the Chinese Academy of Sciences, China). The sensors were spin-coated with casting solution at 1500 rpm for 15 s and then the rotation speed was increased to 8000 rpm for 60 s, followed by drying at 60 °C for 60 min [30]. For preparation of Nafion-coated sensor crystals, the pure Nafion resin was first obtained by evaporation of 5 wt% Nafion solution (DuPont Fluoroproducts, USA) at 100 °C under vacuum for 24 h until dry, then treated by heating at 80 °C in a solution of 3 wt % $H_2O_2$, deionized water, 0.5 M $H_2SO_4$ and deionized water, each for 1 h [31]. A homogeneous Nafion solution was prepared by dissolving Nafion resin in DMAc. The remaining steps were the same as above.

All QCM-D experiments were performed under flow-through conditions using a peristaltic pump (Ismatec, Switzerland) at 100 μL/min flow rate. The temperature was maintained at 23 °C. Prior to each QCM-D experiment, a baseline with UP was acquired. BSA solutions were injected sequentially to the QCM-D system in the following order: (i) background solution of either UP or 50 mM PBS; (ii) 10 mg/L of BSA as dissolved organic content (DOC) dissolved in the background solution; and (iii) a similar background solution to (ii) without BSA. The variations in frequency and dissipation factor were measured for the three overtones ($n$=3, 5, and 7), but only data from the third overtone are presented.

### 2.4. MFC construction and operation

Two cubic chambers were constructed from Plexiglas and separated by a PEM. The volume of each chamber was 165 ml with a working volume of 150 ml. Carbon felts (Fengxiang Science & Technology Co., Ltd, China) with a thickness of 5 mm were selected as the electrodes. The anode and the cathode were cut into rectangles having a projected surface area of 9 $cm^2$ and 12 $cm^2$, respectively. The carbon felts were pretreated by washing in 1 M HCL and 1 M NaOH, each for 24 h, and rinsed with deionized water to remove possible trace metal and biomass contamination [32]. Air was continuously purged into the cathode chamber using an air pump.

The MFCs were inoculated with anaerobic wastewater from the Xi'an fourth sewage treatment plant. The anode medium contained (per L): 1.64 g sodium acetate, 4.58 g $Na_2HPO_4$, 2.45 g $NaH_2PO_4$, 0.31 g $NH_4Cl$, 0.13 g KCl, and 12.5 ml trace minerals [33]. The cathode chamber contained a 50 mM phosphate buffer solution. The external resistance was fixed at 1000 Ω and all reactors were operated in fed-batch mode at a temperature of 30 ± 1 °C. The anode solution was replaced when the voltage dropped below 30 mV.

The voltages ($E$) across the external resistance ($Rex$) were recorded every 2 min using a data acquisition system (SIN-R200D, Sinomeasure Automation Technology Co., Ltd, China). Current ($I$) was calculated using Ohm's law according to $I=E/Rex$. Power densities were calculated as $P=IE$. The current and power were normalized by the projected surface area of the membrane. After the MFCs generated power stably, the polarization and power density curves were obtained by varying the external resistance from 10 to 9000 Ω over a single cycle [34]. The total internal resistance was determined from the linear portion of the polarization data using the polarization slope method [35]. Total chemical oxygen demand (COD) was measured using standard methods. The evaluated coulombic efficiency ($CE$) over time was calculated using:

$$CE = \frac{M\int_0^t Idt}{FbV_{an}\Delta COD}, \tag{4}$$

where $M$ is the molecular weight of oxygen (32), $F$ is the Faraday constant, $b$ is the number of electrons exchanged per molecule of oxygen (4 in this case), $V_{an}$ is the volume of liquid in the anode compartment, and ΔCOD is the change in COD over time $t$.

Nafion 117 was pretreated by sequentially boiling in $H_2O_2$ (3%), deionized water, 0.5 M $H_2SO_4$, and then deionized water (each time for 1 h).

## 3. Results and discussion

The role of BPO in the graft reactions and the processes of ozone preactivation of PVDF and graft copolymerization of SSS are illustrated schematically in Fig. 1. Peroxide and hydroperoxide species with high activity can be generated on PVDF main chains by ozone preactivation, which require less activation energy of reacting with the free radicals generated by the BPO pyrolysis compared to that of directly generating active sites on PVDF by the free radicals. Thereby, the active sites used for graft reactions were increased and the grafting efficiency of SSS on PVDF main chains was greatly improved.

### 3.1. FTIR analysis of PVDF-g-PSSA membrane

The FTIR analysis was conducted to demonstrate the success of the grafting processes. Fig. 2 shows the FTIR analysis of PVDF-g-PSSA membrane and PVDF membrane. For PVDF membrane, the peak at 488 $cm^{-1}$ is attributed to C–F bending vibration. The peak at 1408 $cm^{-1}$ corresponds to the characteristic absorption bond of PVDF. The peaks at 2983 $cm^{-1}$ and 3024 $cm^{-1}$ correspond to the symmetric and asymmetric stretching vibrations of $CH_2$ group, respectively. Compared with

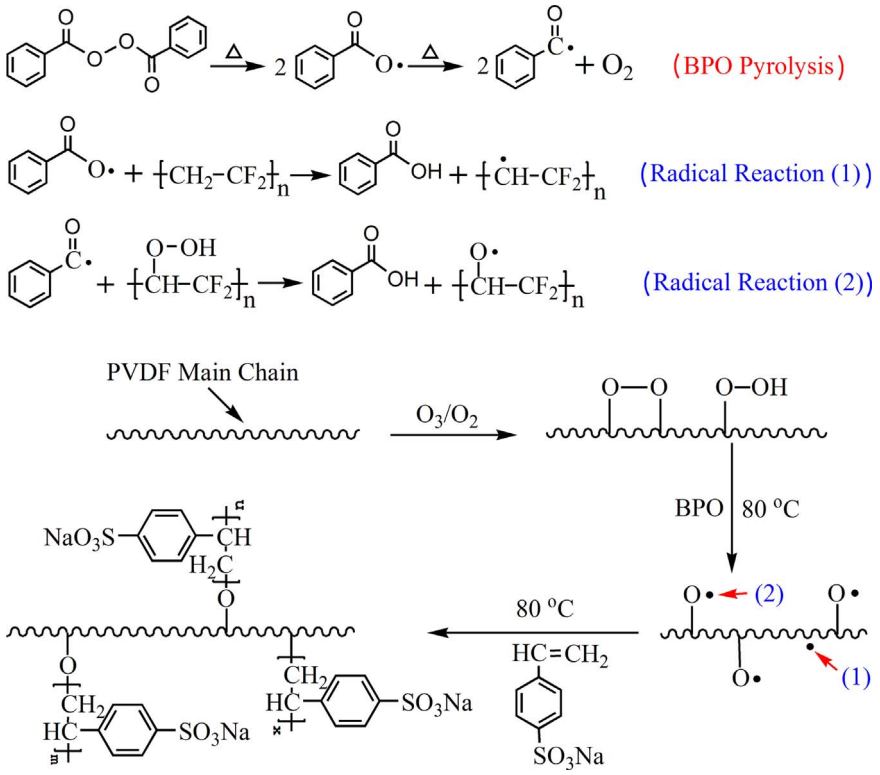


**Fig. 1.** Schematic illustration of the processes of ozone pretreatment of PVDF and graft copolymerization of SSS.

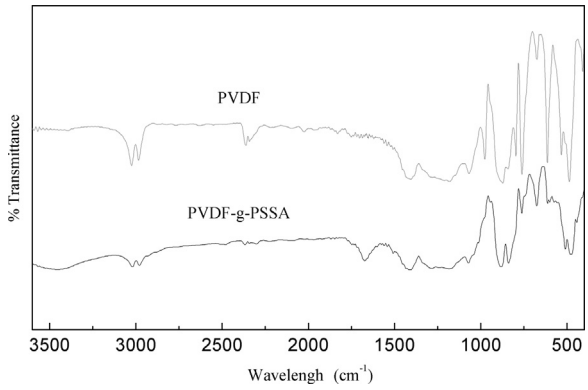


**Fig. 2.** FTIR spectra of PVDF membrane and PVDF-g-PSSA membrane.

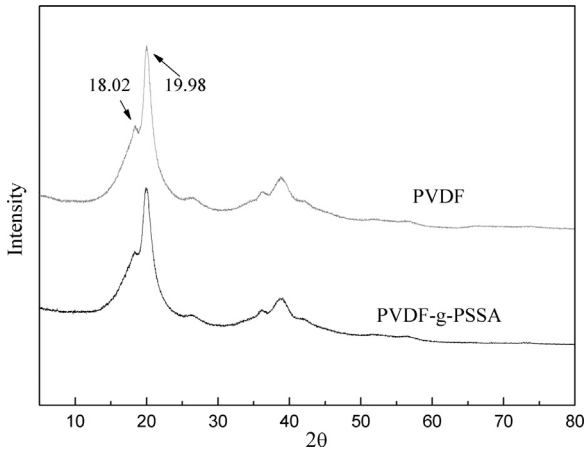


**Fig. 3.** XRD diffraction curves of PVDF membrane and PVDF-g-PSSA membrane.

the PVDF membrane, the presence of skeletal C=C in-plane stretching vibrations at 1560 and 1672 $cm^{-1}$ demonstrates the presence of aromatic ring features. The peaks at 1068 and 1280 $cm^{-1}$ are caused by the presence of $SO_3^-$ groups. The broad peak at 3549 $cm^{-1}$ is attributed to the water molecules incorporated in the hydrophilic sulfonated material [19,20]. These new peaks indicate that SSS was successfully grafted onto PVDF and the PVDF-g-PSSA membranes were obtained.

### 3.2. XRD analysis of PVDF-g-PSSA membrane

The crystalline structure and the crystallinity of PVDF membranes have an important influence on the proton conductivity and thermal stability of PVDF-g-PSSA membranes. In the present work, the effect of grafting SSS on the crystalline morphology of PVDF membranes was studied with XRD. Fig. 3 shows the diffraction patterns of PVDF-g-PSSA membrane and PVDF membrane. The PVDF-g-PSSA membrane has a similar crystalline structure to that of the PVDF membrane. The crystalline peak positions at angles of $2\theta$=18.02° and $2\theta$=19.98° do not indicate an obvious shift. However, the overall crystalline peak area of the PVDF-g-PSSA membrane decreased. These results suggest a decrease in the crystallinity of the membranes and are attributed to the dilution of the structure with the amorphous poly(styrene sulfonic acid) grafts. It can be concluded that the grafts are initiated from the amorphous region of the PVDF matrix and do not disrupt the inherent crystallites during the grafting process. These observations are consistent with the findings of previous studies on grafting of SSS or styrene onto PVDF membranes [19,36].

### 3.3. TGA of PVDF-g-PSSA membrane

The thermal stability of the PVDF-g-PSSA membrane was evaluated by thermal gravity analysis and was compared to that of the pristine PVDF membrane in Fig. 4. The onset of the major weight loss of the PVDF-g-PSSA membrane occurs at about 450 °C, higher than that of the PVDF membrane, which is due to the larger molecular weight of the PVDF-g-PSSA membrane because of SSS grafted onto PVDF main

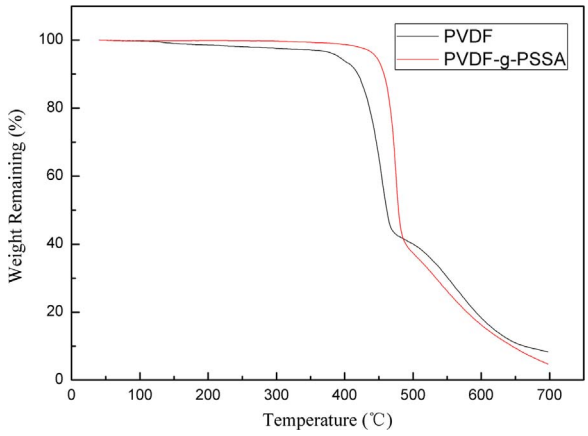


**Fig. 4.** Thermal gravity analysis curves of PVDF membrane and PVDF-g-PSSA membrane.

chains. While, the PVDF-g-PSSA membrane presents a greater weight loss compared to that of the PVDF membrane, associated with the thermal decomposition of the PSSA segments. It was demonstrated that SSS was successfully grafted onto PVDF main chains, rather than a simple blending of the two species. The PVDF-g-PSSA membrane has excellent thermal stability.

### 3.4. Membrane properties

The degree of grafting of the PVDF-g-PSSA copolymer and the physical and electrochemical properties of the prepared membranes were examined and are listed in Table 1.

The degree of grafting increases with the increase in SSS monomer concentration used for graft copolymerization; this is attributed to the increase in the number of sulfonate groups in the polymer. Graft copolymerization with the ozone preactivation method depends on the initiator concentration in the PVDF chains and the concentration of the monomer molecules available at the graft sites. It can be assumed that more SSS molecules will be grafted onto PVDF chains as the SSS monomer concentration in the graft mixture increases, because of the increased availability of SSS molecules at the grafting sites, which results in an increase in the number of sulfonic acid groups in the polymer [18,20,37]..

The water uptake increases with the increase of the degree of grafting, which is attributed to more sulfonate groups grafted onto the polymer membranes. When the degree of grafting was 50.52%, the water uptake of the prepared membrane was 25%, which was close to that of Nafion 117 membrane (20%). Compared to the membrane prepared in the present work, the water uptake of membranes reported by Lehtinen et al. [16]. and Nasef et al. [20] reached 115% and 71%, respectively, at about the similar degree of grafting. The water uptake of the proton exchange membrane is affected by the content of the ion-exchange groups contained in the membrane and the microstructure of the membrane. The total water uptake of membrane typically includes water molecules tightly to the ion-exchange groups and the water adsorbed in the membrane pores. Since the methods used in these papers differ from that described in the present work, the membranes prepared have different microstructures. Larger pores accompanied higher water uptake and conductivity [38]. The water uptake values of membrane prepared by Lehtinen et al. and Nasef et al. are close to or greater than 100%, which means that most of the membrane weight should be due to adsorption of large amounts of water in the membrane pores [16]. Besides, the membranes were boiled in water for 1 h before measurements in Lehtinen's work, which resulted in a greater degree of swelling of the membrane to adsorb more water.

The change in the membrane-swelling ratio has a similar trend to that of the water uptake, namely a slight increase in the swelling ratio with increases in SSS monomer concentration used for graft copolymerization. The swelling ratio has a positive correlation with the number of sulfonic acid groups in the membranes. The breaking strength of the PVDF-g-PSSA membranes was slightly higher than that of the PVDF membrane, indicating that the prepared membranes retain the excellent mechanical properties of PVDF. When the degree of grafting was 50.52%, the breaking strength of the prepared membrane reached 28.63 MPa, which was higher than that of Nafion 117 (15.08 MPa). The low swelling ratio and high breaking strength are favorable for practical application of the PVDF-g-PSSA membranes.

The contact angle of the membranes was found to decrease as the SSS monomer concentration increased. The contact angle of the original PVDF membranes was 101.28° while the contact angle of the PVDF-g-PSSA membranes reached 79.86° when the degree of grafting was 50.52%. These observations are consistent with the findings of previous studies on SSS grafted onto PVDF porous membranes by an electron beam-initiated surface grafting method [39]. The ionic character of the grafting chains plays an important role in decreasing the contact angles. The hydrophilicity of the PVDF-g-PSSA membranes increases significantly as more SSS monomer is incorporated in the PVDF membranes because of the increase in the number of sulfonate groups in the membranes. The contact angle measurements are further proof of the successful grafting of SSS onto the PVDF membranes and are in agreement with the FTIR and XRD results for the grafted and unmodified PVDF membranes.

The proton conductivity of the proton exchange membrane is one of the factors most affecting the performance of the MFCs. It is determined by the water uptake in the membrane and the number of ion-exchange groups in the grafting chains [40,41]. As expected, increasing the SSS monomer concentration in the graft mixture increases the proton conductivity of the PVDF-g-PSSA membranes. As the ion-exchange groups in polymer increase, the water uptake of the membrane and the number of water molecules per exchange site increase, which are conducive to the increase of the proton conductivity. The conductivity is also dependent on the degree of crystallinity [20,42]. As explained in Section 3.2, the degree of crystallinity of the PVDF-g-PSSA

**Table 1**
Degree of grafting of the PVDF-g-PSSA copolymer and the physical and electrochemical properties of the membranes prepared with different mass ratio of PVDF/SSS.

| Mass ratio of PVDF/SSS | Degree of grafting (%) | Physical and electrochemical properties of the membranes | | | | |
|---|---|---|---|---|---|---|
| | | Water uptake (%) | Swelling ratio (%) | Breaking strength (MPa) | Contact angle (°) | Proton conductivity (S/cm) |
| 1:0 | – | 5.00 | 2.56 | 25.89 | 101.283 | 0.000 |
| 1:1 | 20.62 | 18.18 | 5.00 | 26.02 | 86.052 | 0.010 |
| 1:2 | 32.99 | 20.52 | 6.16 | 28.49 | 85.908 | 0.021 |
| 1:3 | 41.24 | 22.60 | 6.56 | 28.55 | 83.446 | 0.032 |
| 1:4 | 46.39 | 23.81 | 7.37 | 28.57 | 81.582 | 0.037 |
| 1:5 | 50.52 | 25.00 | 7.78 | 28.63 | 79.865 | 0.046 |

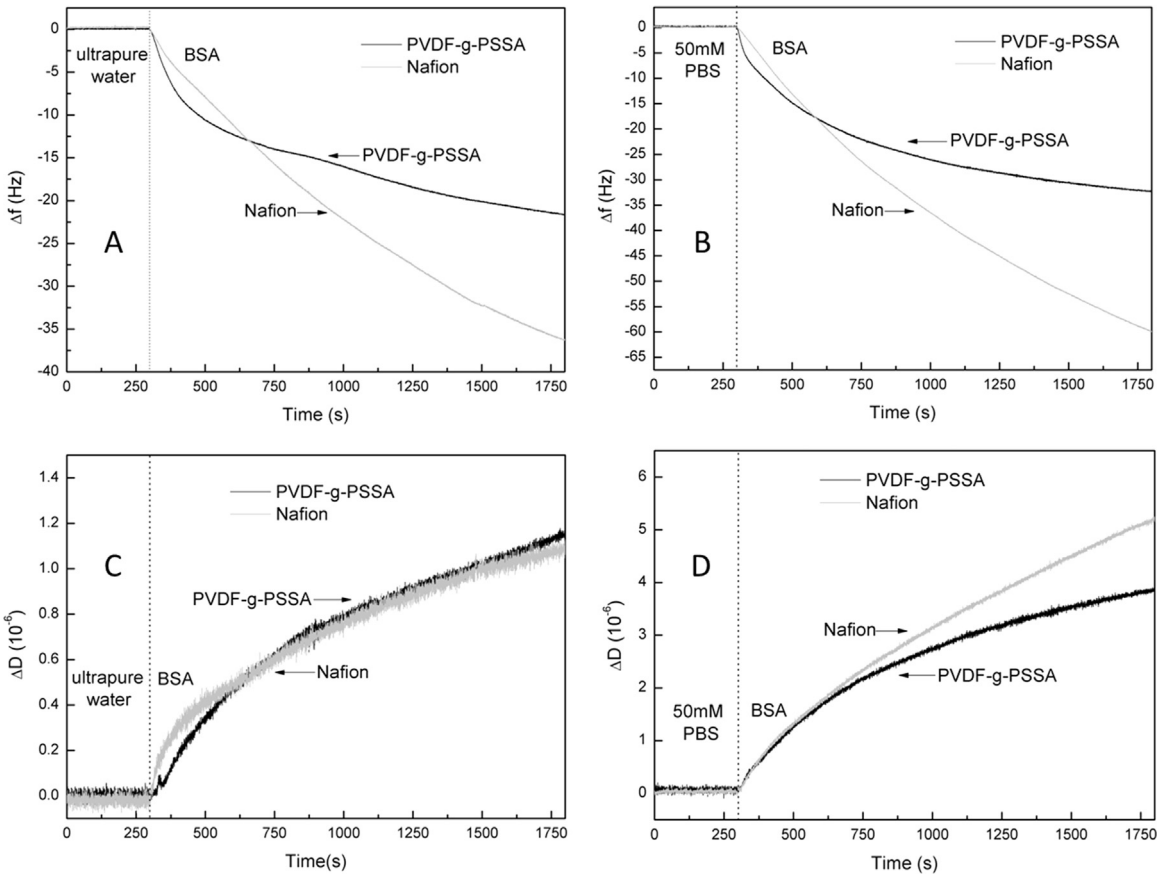


**Fig. 5.** Frequency (Δ*f*) and dissipation (Δ*D*) responses from the adsorption of BSA on two different membrane-coated sensors: (A, C) BSA dissolved in ultrapure water; (B, D) BSA dissolved in 50 mM PBS.

membranes decreases, which may contribute to the increase of proton conductivity. The proton conductivity of the PVDF-g-PSSA membranes reached 0.046 S/cm when the degree of grafting was 50.52%, which is close to that of Nafion 117 (0.078 S/cm) [29,43] and was used in the MFC study. All of these results indicate that the PVDF-g-PSSA membranes have excellent conductive properties.

### 3.5. Analysis of adherence and viscoelastic properties with QCM-D

The adsorption behavior of BSA on both the PVDF-g-PSSA- and Nafion-coated sensor surfaces and the structural changes of the corresponding BSA adsorbed layers were investigated in the presence of either UP or 50 mM PBS solution. The 50 mM PBS solution was chosen because it is the most commonly used buffer solution in MFC. Representative time-resolved QCM-D measurement parameter shifts are presented in Fig. 5, revealing the frequency (Δ*f*) and dissipation (Δ*D*) at the third overtone under the two water conditions. The frequency shift of the PVDF-g-PSSA-coated sensor crystal was smaller than that of the Nafion-coated sensor crystal in the presence of either UP or 50 mM PBS solution, in spite of a slower adsorption of BSA on the Nafion-coated crystal in the initial stage (Fig. 5A, C). From the Sauerbrey relation ($\Delta m = -C \cdot \Delta f / n$), in which $C$ is the Sauerbrey constant for the 5 MHz resonance frequency and $n$ is the overtone number, the accumulated mass (Δ*m*) on the sensor crystal surface was proportional to the measured Δ*f* shift. It is clear that the amount of BSA on the Nafion surface was more than that on the PVDF-g-PSSA surface in the presence of either UP or 50 mM PBS because of the hydrophobic properties of the Nafion membrane, which demonstrated that our PVDF-g-PSSA membrane showed superior antifouling performance to that of the Nafion membrane.

Compared with the extent of frequency shift of BSA adsorbed on the membrane-coated crystal in the presence of UP, Δ*f* showed more substantial changes in 50 mM PBS. That is, more BSA will adsorb and accumulate onto both membrane surfaces in the presence of 50 mM PBS. From the classical Derjaguin–Landau–Verwey–Overbeek (DLVO) theory, it is likely that in the presence of 50 mM PBS, the charges of the membrane surface and BSA are significantly shielded, because of electric double layer compression and charge screening, leading to a decrease in electrostatic repulsion between the membrane surface and the adsorbed BSA film. Consequently, the enhanced deposition rate of BSA is represented by the higher frequency and dissipation shifts of the membrane-coated crystal [44]. In the MFC, because of the large quantities of cations in the PBS solution, the sulfonate groups in the cation exchange membrane were occupied by these cations rather than protons, which will result in a decrease in the membrane conductivity and the increase of membrane resistance.

During the long-term operation of an MFC, biofouling will occur and a biofilm layer will form on the membrane surface. Biofouling is caused by organic foulants and biofoulants. Besides, intermolecular bridging by cations in the PBS buffer solutions between biofoulants and the fouling layer eventually contributes to the formation of a strong fouling layer on the membrane. Biofilms will cause physical blockage of cation transfer and a significant increase in membrane resistance, eventually reducing MFC performance. These results were consistent with the QCM-D results, which indicated that more BSA was adsorbed on the membrane surface in PBS solution than in ultrapure water.

To gain further insight into the nature of the adsorbed BSA layers on the membrane surface, the structural properties of the deposited BSA were analyzed by examining Δ*D* with respect to the overall Δ*f*. The final $|\Delta D/\Delta f|$ ratio could be used to compare the structural characteristics of the BSA layer on different membranes, with lower $|\Delta D/\Delta f|$

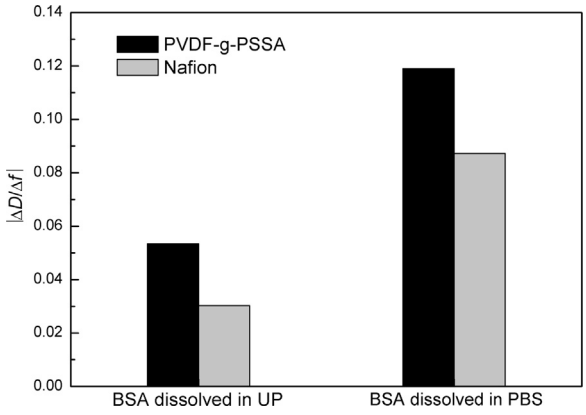


**Fig. 6.** $|\Delta D/\Delta f|$ data plots for BSA adsorption on two different membrane-coated sensors in either UP or PBS solution.

values indicative of a less hydrated or compact protein layer [45]. The final $|\Delta D/\Delta f|$ ratios for BSA adsorbed onto membrane-coated sensors in the presence of either UP or 50 mM PBS solution are presented in Fig. 6. It is clear that BSA adsorption on the PVDF-g-PSSA membrane demonstrated higher $|\Delta D/\Delta f|$ values under the two water conditions, indicating that the BSA layer deposited on the Nafion surface became more compact. The higher $|\Delta D/\Delta f|$ values in 50 mM PBS solution compared with those in UP suggested that a nonrigid and open-structure BSA layer was formed on the membrane surface where cations existed. Therefore, it was easier to form a dense layer of fouling on the Nafion membrane surface and the self-made PVDF-g-PSSA membrane had an advantage in antifouling characteristics.

### 3.6. Power density and polarization curves

The power densities obtained for the MFCs with different membranes are presented in Fig. 7. It can be seen that the maximum power density produced by the MFC with PVDF-g-PSSA membrane was 106.7 mW/m$^2$, while the MFC with Nafion 117 produced a maximum power density of 132.0 mW/m$^2$. The power output in the MFC with PVDF-g-PSSA membrane was thus 19.2% less than that of the MFC using Nafion 117 as the proton exchange membrane.

The polarization curves of the MFCs are also shown in Fig. 7. The internal resistances of the MFCs were obtained from the slopes of the polarization data. As shown, the internal resistances of the MFCs with PVDF-g-PSSA membrane and Nafion 117 were 244 Ω and 211 Ω, respectively. The internal resistance in an MFC consists of three components: ohmic resistance of the electrolyte, electrode materials, and membranes; charge transfer resistance; and diffusion resistance

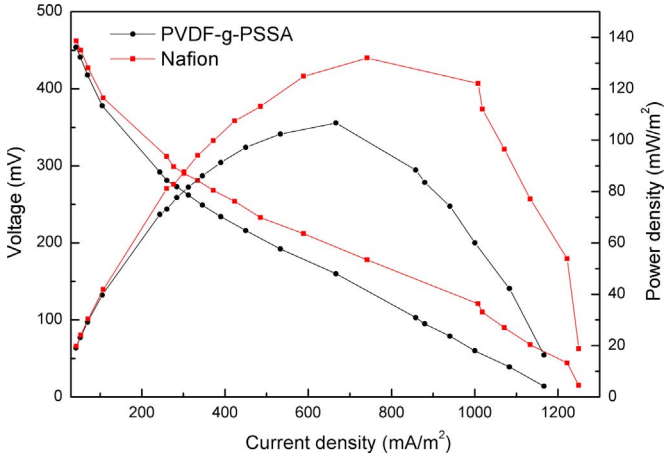


**Fig. 7.** Power density and polarization curve of Nafion 117 and PVDF-g-PSSA membranes in microbial fuel cells.

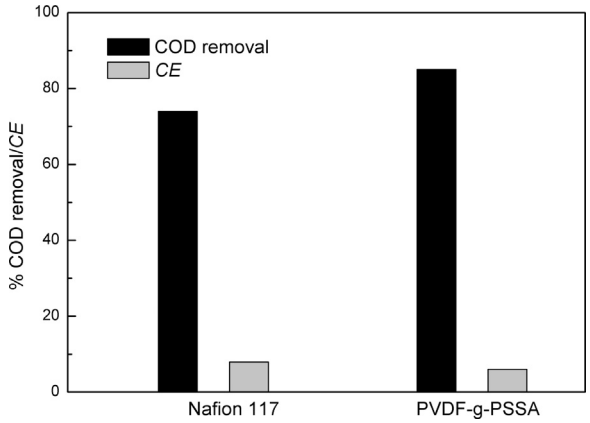


**Fig. 8.** COD removal and *CE* of the Nafion 117 and PVDF-g-PSSA membranes in MFC system.

[46]. In this study, the two MFC reactors had the same configuration and identical substrates. Therefore, the difference in internal resistances of the two systems with different membranes was most likely derived from the membranes. As described above, Nafion 117 shows a higher conductivity than PVDF-g-PSSA. Although the power production in the MFC with PVDF-g-PSSA membrane was less than that in the Nafion 117 MFC, it still has a strong possibility of being used in MFCs because of its lower costs and more simplified preparation process.

### 3.7. COD removal and CE

The COD removal and *CE* of the MFCs with different membranes are shown in Fig. 8. COD removal was high ( > 70%) for all systems. The MFC with Nafion 117 had 74% COD removal, while the MFC with PVDF-g-PSSA membrane had a much higher COD removal of 85%. Taking into account its lower power density of the MFC with PVDF-g-PSSA membrane (Fig. 7), its much higher COD removal indicated that more substrate was used by anaerobic digestion, rather than for electricity production. The *CE* percentages of the MFCs using Nafion 117 and the PVDF-g-PSSA membrane were 7.90% and 5.96%, respectively. Both systems showed low coulombic efficiency, mainly because of the high substrate concentration used in the MFCs and the absence of a cathode catalyst. The higher substrate concentration required longer times to degrade the substrate fully, which resulted in more oxygen leakage into the system, causing substrate loss by aerobic removal of microorganisms, and lowering the overall *CE* [47]. The MFC with Nafion 117 had higher *CE*, possibly because of its lower internal resistance compared with that of the system with the PVDF-g-PSSA membrane.

## 4. Conclusions

PVDF-g-PSSA proton exchange membranes were prepared successfully using a new method. The PVDF-g-SSS copolymer was first produced via thermally induced graft copolymerization of SSS with ozone-preactivated PVDF. Then, sulfonic acid proton exchange membranes were prepared using a solvent evaporation method. The proton conductivity of the membranes depends on the concentration of SSS monomer in the graft mixture. The PVDF-g-PSSA proton exchange membrane possesses high proton conductivity and was applied successfully as a high-performance and less expensive separator in MFCs compared with Nafion 117. Our PVDF-g-PSSA membrane showed superior antifouling characteristics to those of Nafion membrane, and the Nafion membrane surface formed a dense fouling layer more easily. Taking into account its lower cost and excellent proton conductivity, our PVDF-g-PSSA membrane is a promising candidate for use as the separator in MFCs.

## Acknowledgements

Financial support for this study was provided by the Innovative Research Team of Xi'an University of Architecture and Technology, the National Natural Science Foundation of China (Grant Nos. 51278408) and the Shanxi Province Science and Technology Youth Star Project (Grant Nos. 2014KJXX-65).

## References

[1] D.P. Strik, H. Terlouw, H.V. Hamelers, C.J. Buisman, Renewable sustainable biocatalyzed electricity production in a photosynthetic algal microbial fuel cell (PAMFC), Appl. Microbiol. Biotechnol. 81 (2008) 659–668.
[2] S. Shafiee, E. Topal, When will fossil fuel reserves be diminished?, Energy Policy 37 (2009) 181–189.
[3] B.E. Logan, Exoelectrogenic bacteria that power microbial fuel cells, Nat. Rew. Microbiol. 7 (2009) 375–381.
[4] X. Xie, L. Hu, M. Pasta, G.F. Wells, D. Kong, C.S. Criddle, Y. Cui, Three-dimensional carbon nanotube-textile anode for high-performance microbial fuel cells, Nano Lett. 11 (2011) 291–296.
[5] S.-E. Oh, S. Van Ginkel, B.E. Logan, The relative effectiveness of pH control and heat treatment for enhancing biohydrogen gas production, Environ. Sci. Technol. 37 (2003) 5186–5190.
[6] Z. Ge, Q. Ping, L. Xiao, Z. He, Reducing effluent discharge and recovering bioenergy in an osmotic microbial fuel cell treating domestic wastewater, Desalination 312 (2013) 52–59.
[7] C.J. Sund, S. McMasters, S.R. Crittenden, L.E. Harrell, J.J. Sumner, Effect of electron mediators on current generation and fermentation in a microbial fuel cell, Appl. Microbiol. Biotechnol. 76 (2007) 561–568.
[8] Q. Deng, X. Li, J. Zuo, A. Ling, B.E. Logan, Power generation using an activated carbon fiber felt cathode in an upflow microbial fuel cell, J. Power Sources 195 (2010) 1130–1135.
[9] K.J. Chae, M. Choi, F.F. Ajayi, W. Park, I.S. Chang, I.S. Kim, Mass transport through a proton exchange membrane (Nafion) in microbial fuel cells†, Energy Fuels 22 (2008) 169–176.
[10] T.H. Choi, Y.-B. Won, J.-W. Lee, D.W. Shin, Y.M. Lee, M. Kim, H.B. Park, Electrochemical performance of microbial fuel cells based on disulfonated poly(-arylene ether sulfone) membranes, J. Power Sources 220 (2012) 269–279.
[11] J. Xu, G.P. Sheng, H.W. Luo, W.W. Li, L.F. Wang, H.Q. Yu, Fouling of proton exchange membrane (PEM) deteriorates the performance of microbial fuel cell, Water Res. 46 (2012) 1817–1824.
[12] M. Miskan, M. Ismail, M. Ghasemi, J. Md Jahim, D. Nordin, M.H. Abu Bakar, Characterization of membrane biofouling and its effect on the performance of microbial fuel cell, Int. J. Hydrog. Energy 41 (2016) 543–552.
[13] L. Nguyen, F. Mighri, Y. Deyrail, S. Elkoun, Conductive materials for proton exchange membrane fuel cell bipolar plates made from PVDF, PET and co-continuous PVDF/PET filled with carbon additives, Fuel Cells 10 (2010) 938–948.
[14] G.K.S. Prakash, M.C. Smart, Q.-J. Wang, A. Atti, V. Pleynet, B. Yang, K. McGrath, G.A. Olah, S.R. Narayanan, W. Chun, T. Valdez, S. Surampudi, High efficiency direct methanol fuel cell based on poly(styrenesulfonic) acid (PSSA)–poly(vinylidene fluoride) (PVDF) composite membranes, J. Fluor. Chem. 125 (2004) 1217–1230.
[15] M.M. Nasef, N.A. Zubir, A.F. Ismail, M. Khayet, K.Z.M. Dahlan, H. Saidi, R. Rohani, T.I.S. Ngah, N.A. Sulaiman, PSSA pore-filled PVDF membranes by simultaneous electron beam irradiation: preparation and transport characteristics of protons and methanol, J. Membr. Sci. 268 (2006) 96–108.
[16] T. Lehtinen, G. Sundholm, S. Holmberg, F. Sundholm, P. Bjornbomd, M. Bursell, Electrochemical characterization of PVDF-based proton conducting membranes for fuel cells, Electrochim. Acta 43 (1998) 1881–1890.
[17] X. Qiu, W. Li, S. Zhang, H. Liang, W. Zhu, The microstructure and character of the PVDF-g-PSSA membrane prepared by solution grafting, J. Electrochem. Soc. 150 (2003) A917–A921.
[18] M. Mahmoud Nasef, H. Saidi, K.Z. Mohd Dahlan, Kinetic investigations of graft copolymerization of sodium styrene sulfonate onto electron beam irradiated poly(vinylidene fluoride) films, Radiat. Phys. Chem. 80 (2011) 66–75.
[19] M.M. Nasef, H. Saidi, K.Z.M. Dahlan, Acid-synergized grafting of sodium styrene sulfonate onto electron beam irradiated-poly(vinylidene fluoride) films for preparation of fuel cell membrane, J. Appl. Polym. Sci. 118 (2010) 2801–2809.
[20] M.M. Nasef, H. Saidi, K.Z.M. Dahlan, Single-step radiation induced grafting for preparation of proton exchange membranes for fuel cell, J. Membr. Sci. 339 (2009) 115–119.
[21] G. Zhai, E.T. Kang, K.G. Neoh, Poly(2-vinylpyridine)- and poly(4-vinylpyridine)-graft-poly(vinylidene fluoride) copolymers and their pH-sensitive microfiltration membranes, J. Membr. Sci. 217 (2003) 243–259.
[22] M. Rahimabady, L.Q. Xu, S. Arabnejad, K. Yao, L. Lu, V.P. Shim, K.G. Neoh, E.-T. Kang, Poly(vinylidene fluoride-co-hexafluoropropylene)-graft-poly(dopamine methacrylamide) copolymers: a nonlinear dielectric material for high energy density storage, Appl. Phys. Lett. 103 (2013) 262904.
[23] E.T. Kang, Y. Zhang, Surface modification of fluoropolymers via molecular design, Adv. Mater. 12 (2000) 1481–1494.
[24] B. Deng, X. Yang, L. Xie, J. Li, Z. Hou, S. Yao, G. Liang, K. Sheng, Q. Huang, Microfiltration membranes with pH dependent property prepared from poly(-methacrylic acid) grafted polyethersulfone powder, J. Membr. Sci. 330 (2009) 363–368.
[25] S.-J. Seo, B.-C. Kim, K.-W. Sung, J. Shim, J.-D. Jeon, K.-H. Shin, S.-H. Shin, S.-H. Yun, J.-Y. Lee, S.-H. Moon, Electrochemical properties of pore-filled anion exchange membranes and their ionic transport phenomena for vanadium redox flow battery applications, J. Membr. Sci. 428 (2013) 17–23.
[26] S.-H. Yun, J.-J. Woo, S.-J. Seo, L. Wu, D. Wu, T. Xu, S.-H. Moon, Sulfonated poly(2,6-dimethyl-1,4-phenylene oxide) (SPPO) electrolyte membranes reinforced by electrospun nanofiber porous substrates for fuel cells, J. Membr. Sci. 367 (2011) 296–305.
[27] H. Susanto, M. Ulbricht, Characteristics, performance and stability of polyether-sulfone ultrafiltration membranes prepared by phase separation method using different macromolecular additives, J. Membr. Sci. 327 (2009) 125–135.
[28] T.A. Zawodzinski, M. Neeman, L.O. Sillerud, S. Gottesfeld, Determination of water diffusion coefficients in perfluorosulfonate ionomeric membranes, J. Phys. Chem. 95 (1991) 6040–6044.
[29] M. Gil, X. Ji, X. Li, H. Na, J. Eric Hampsey, Y. Lu, Direct synthesis of sulfonated aromatic poly(ether ether ketone) proton exchange membranes for fuel cell applications, J. Membr. Sci. 234 (2004) 75–81.
[30] R. Miao, L. Wang, N. Mi, Z. Gao, T. Liu, Y. Lv, X. Wang, X. Meng, Y. Yang, Enhancement and mitigation mechanisms of protein fouling of ultrafiltration membranes under different ionic strengths, Environ. Sci. Technol. 49 (2015) 6574–6580.
[31] C. Bi, H. Zhang, Y. Zhang, X. Zhu, Y. Ma, H. Dai, S. Xiao, Fabrication and investigation of $SiO_2$ supported sulfated zirconia/Nafion® self-humidifying membrane for proton exchange membrane fuel cell applications, J. Power Sources 184 (2008) 197–203.
[32] Z. Wang, J. Ma, Y. Xu, H. Yu, Z. Wu, Power production from different types of sewage sludge using microbial fuel cells: a comparative study with energetic and microbiological perspectives, J. Power Sources 235 (2013) 280–288.
[33] D.R. Lovley, E.J. Phillips, Novel mode of microbial energy metabolism: organic carbon oxidation coupled to dissimilatory reduction of iron or manganese, Appl. Environ. Microbiol. 54 (1988) 1472–1480.
[34] Y. Ahn, B.E. Logan, Altering anode thickness to improve power production in microbial fuel cells with different electrode distances, Energy Fuels 27 (2012) 271–276.
[35] B.E. Logan, Microbial Fuel Cells, John Wiley & Sons, New York, 2008.
[36] S. Hietala, M. Paronen, S. Holmberg, J. Näsman, J. Juhanoja, M. Karjalainen, R. Serimaa, M. Toivola, T. Lehtinen, K. Parovuori, Phase separation and crystallinity in proton conducting membranes of styrene grafted and sulfonated poly(-vinylidene fluoride), J. Polym. Sci., Part A: Polym. Chem. 37 (1999) 1741–1753.
[37] T. Cai, K. Neoh, E. Kang, S. Teo, Surface-functionalized and surface-functionalizable poly(vinylidene fluoride) graft copolymer membranes via click chemistry and atom transfer radical polymerization, Langmuir 27 (2011) 2936–2945.
[38] N. Walsby, S. Hietala, S.L. Maunu, F. Sundholm, T. Kallio, Gr Sundholm, Water in different poly(styrene sulfonic acid)-grafted fluoropolymers, J. Appl. Polym. Sci. 86 (2002) 33–42.
[39] F. Liu, B.-K. Zhu, Y.-Y. Xu, Improving the hydrophilicity of poly(vinylidene fluoride) porous membranes by electron beam initiated surface grafting of AA/SSS binary monomers, Appl. Surf. Sci. 253 (2006) 2096–2101.
[40] Y. Xue, F.U. Rongqiang, Preparation of speek and speek/chitosan composite proton-exchange membranes for application in direct methanol fuel cells, Acta Polym. Sin. 010 (2010) 285–291.
[41] W. Jang, S. Sundar, S. Choi, Y.-G. Shul, H. Han, Acid–base polyimide blends for the application as electrolyte membranes for fuel cells, J. Membr. Sci. 280 (2006) 321–329.
[42] S. Holmberg, T. Lehtinen, J. Näsman, D. Ostrovskii, M. Paronen, R. Serimaa, F. Sundholm, G. Sundholm, L. Torell, M. Torkkeli, Structure and properties of sulfonated poly [(vinylidene fluoride)–g-styrene] norous membranes porous membranes, J. Mater. Chem. 6 (1996) 1309–1317.
[43] Y. Sone, P. Ekdunge, D. Simonsson, Proton conductivily of Nafion 117 as measured by a four-electrode AC impedance method, J. Electrochem. Soc. 143 (1996) 1254–1259.
[44] Y. Wang, Y. Fei, A. Bick, G. Oron, M. Herzberg, Extracellular polymeric substances (EPS) in a hybrid growth membrane bioreactor (HG-MBR): viscoelastic and adherence characteristics, Environ. Sci. Technol. 44 (2010) 8636–8643.
[45] X. Chang, D.C. Bouchard, Multiwalled carbon nanotube deposition on model environmental surfaces, Environ. Sci. Technol. 47 (2013) 10372–10380.
[46] Z. He, F. Mansfeld, Exploring the use of electrochemical impedance spectroscopy (EIS) in microbial fuel cell studies, Energy Environ. Sci. 2 (2009) 215–219.
[47] H. Liu, S. Cheng, B.E. Logan, Production of electricity from acetate or butyrate using a single-chamber microbial fuel cell, Environ. Sci. Technol. 39 (2005) 658–662.